J. Phys. B: At. Mol. Opt. Phys. 27 (1994) 5221-5239. Printed in the UK

Photoionization of Kr near the 4s threshold: IV. Photoionization through the autoionization of doubly-excited states

B M Lagutin†, V L Sukhorukov†, I D Petrov†, H Schmoranzer‡, A Ehresmann‡ and K-H Schartner§

† Rostov State University of Transport Communications, Rostov-on-Don 344017, Russian Federation

‡ Fachbereich Physik, Universität Kaiserslautern, D-67653 Kaiserslautern, Federal Republic of Germany

§ I Physikalisches Institut, Universität Giessen, D-35392 Giessen, Federal Republic of Germany

Received 6 June 1994, in final form 12 August 1994

Abstract. The photoionization cross sections for the production of the Kr II 4s state and Kr II satellite states were studied in the 4s ionization threshold region. The interference of direct photoionization and ionization through the autoionization decay of doubly-excited states was considered. In the calculations of doubly-excited state energies, performed by a configuration interaction technique, the 4p spin–orbit interaction and the (Kr II core)–(excited electron) Coulomb interaction were included. The theoretical cross sections are in many cases in good agreement with the measured values. Strong resonant features in the satellite spectra with threshold energies greater than 30 eV are predicted.

1. Introduction

A set of recent papers by Schmoranzer *et al* (1993), Sukhorukov *et al* (1994), Ehresmann *et al* (1994) (hereafter referred to as I, II and III, respectively) and the present paper are devoted to the investigation of many-electron processes taking place during the interaction of Kr atoms with exciting photons of energies close to the 4s-electron threshold value. The main intention of these papers is to determine the physical phenomena which cause the complex photon energy dependence of cross sections for the population of the 4s main state and satellite states (Wills *et al* 1990, Schmoranzer *et al* 1990, Hall *et al* 1990).

In I, the absolute values of the cross sections for the production of the 4s main state and several satellite states were measured by the photon-induced fluorescence spectroscopy (PIFS) technique. Many-body calculations of the cross sections for the 4s main state and for most of the even satellite states as well as the oscillator strengths of the transitions into doubly-excited states, performed in the *LS* coupling scheme, have also been presented.

In II, the intermediate-coupling approach was applied for the cross section and oscillator strength calculations. In the framework of this scheme the energetic structure of the Kr II states was calculated, agreeing with the experimental values (Moore 1971)

0953-4075/94/215221+19$19.50

with an accuracy <0.1 eV. The effect of the correlational decrease of the Coulomb interaction between electrons and its influence on the energetic and spectral characteristics of photoionization and photoexcitation into doubly-excited states was considered as well.

Accurate measurements of the Kr 4s photoionization cross section, performed in the extended energy region from the threshold up to 90 eV, were presented in III. Many fine-structure features in the near-threshold region, i.e. ~27.5 to 35 eV, were found and the absolute value of the 4s-electron photoionization cross section in the higher energy region was determined much more precisely than in earlier publications (e.g. Aksela *et al* 1987). In the latter energy region, the measured 4s-electron photoionization cross section is fairly smooth and agrees very well with our calculated values (II). In the near-threshold region, however, the dependence of the 4s-photoionization cross section on the exciting photon energy is of an essentially resonant character. Therefore, the comparison between theory and experiment seemed to be rather difficult in this range, since interference of the direct photoionization channel with the photoionization through the doubly-excited autoionizing states has not been taken into account in the earlier calculations (II). Additionally, in those calculations the interaction of outer electrons in doubly-excited states with the atomic core was taken into account only quite roughly.

The main aim of the present paper is to avoid those approximations and to enable for the first time a comparison of the theoretical and the experimental resonance structures.

2. Theory

Perturbation theory (PT) (Amusia and Cherepkov 1975) was applied in the calculations of the direct photoionization of the Kr atom. The photoionization through the autoionization decay of doubly-excited states was also taken into account. The following scheme describes the processes which were calculated in the present work:

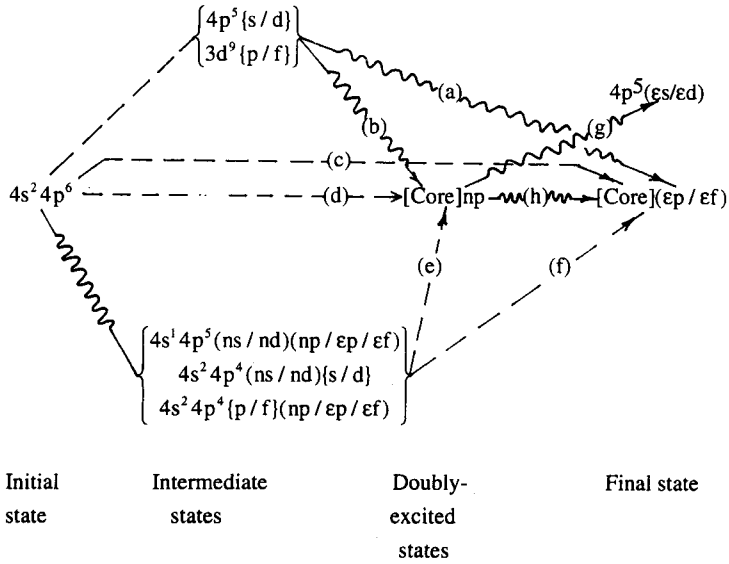

(1)

There are some changes in the scheme (1) with respect to II to describe the transitions through the doubly-excited states. As in II the broken lines denote the electric dipole interaction and the wavy lines the Coulomb interaction of the electrons. The intermediate states $\{l\}$ were summed over the discrete spectrum nl and integrated over the continuous one εl. The notation $(\boldsymbol{a}/\boldsymbol{b})$ means either state $\boldsymbol{a}$ or state $\boldsymbol{b}$ is incorporated in the calculations of the transition amplitude according to the orthogonality conditions. The notation [Core] denotes the Kr II ionic states, which are the superposition of the $4s^14p^6\ ^2S$, $4p^4(L_0S_0)(ns/nd)\ \overline{LS}$ single-configuration basis states.

In scheme (1) the $(a$–$h)$ transitions describe the following processes:

(a, c, f): the direct photoionization of the Kr atom;

(b, d, e): the excitation of the Kr atom into the [Core]np doubly-excited states;

g: The Auger decay of the doubly-excited states into the $4p^5(\varepsilon s/\varepsilon d)$ final states (which do not manifest themselves in the PIFS spectra);

h: the autoionization decay of the doubly-excited states into the [Core]$(\varepsilon p/\varepsilon f)$ final states.

The calculations of energies and wavefunctions of these states as well as amplitudes of the $(a$–$f)$ transitions have been described in II. Therefore, in the present paper only the calculations of energies and wavefunctions of [Core]np doubly-excited states, amplitudes of (g, h) transitions and decays of the [Core]np states taking into account the interference of all transition amplitudes will be described in detail.

2.1. The interference of direct photoionization and photoionization through the autoionization of doubly-excited states

The calculation of photoionization cross sections taking into account the interference of the direct photoionization channels (amplitudes $(a+c+f)$ in scheme (1)) and photoionization through the autoionization of doubly-excited state channels (amplitudes $(b+d+e)\cdot h$ in scheme (1)) presents the problem of interaction of many resonances and many continua. The general aspects of solving this problem were described in the framework of a scattering theory approach (Mies 1968, Starace 1977, Combet-Farnoux 1982). The PT technique, which is used in the present paper, was also applied for the study of this problem (Åberg and Howat 1982).

The N discrete states, characterized by wavefunctions $|n\rangle$ and the B continua with the wavefunctions $|\beta\varepsilon\rangle$ are considered (here ε denotes the energy of an electron in the continuum (in au) and β stands for the quantum numbers of this electron and the core electrons). The $|n\rangle$ and $|\beta\varepsilon\rangle$ wavefunctions are normalized by the following conditions:

$$\langle n|m\rangle = \delta_{n,m} \tag{2}$$

$$\int \langle \beta\varepsilon|\beta'\varepsilon'\rangle \, \mathrm{d}\varepsilon' = \delta_{\beta,\beta'}. \tag{3}$$

According to equation (3) the energetic normalization of continuous wavefunctions with the $(2/\pi)^{1/2}(2\varepsilon)^{-1/4}$ asymptotic behaviour is used and the integration is carried out from zero to infinity.

Both the $|n\rangle$ and $|\beta\varepsilon\rangle$ states are assumed to be prediagonalized which means the fulfilment of the following conditions:

$$\langle n|H|m\rangle = E_n\delta_{n,m} \tag{4}$$

$$\langle \beta\varepsilon|H|\beta'\varepsilon'\rangle = (E_\beta - \varepsilon)\delta_{\beta,\beta'}\delta(\varepsilon-\varepsilon') \tag{5}$$

where E_β is the threshold energy, i.e. the energy of the $|\beta\varepsilon\rangle$ state but with $\varepsilon=0$.

However, the discrete states interact with the continuum via the Hamiltonian H:

$$\langle n|H|\beta\varepsilon\rangle = V_{n\beta} \tag{6}$$

and the ground state $|0\rangle$ is connected with $|n\rangle$ and $|\beta\varepsilon\rangle$ states by the electric dipole transition operator D:

$$\langle n|D|0\rangle = D_n \tag{7}$$

$$\langle \beta\varepsilon|D|0\rangle = D_\beta . \tag{8}$$

It should be noted that the matrix elements $V_{n\beta}$ are real, while D_n and D_β are complex, since in (1) the $(a+c+f)$ and $(b+d+e)\cdot h$ amplitudes are complex.

The states $|\beta\varepsilon\rangle$ in the continua are changed owing to their interaction with the discrete states. In PT the modified wavefunctions $|(\overline{\overline{\beta\varepsilon}})\rangle$ can be determined by the following expression:

$$|(\overline{\overline{\beta\varepsilon}})\rangle = |\beta\varepsilon\rangle + \sum_n^N \frac{V_{n\beta}}{(\varepsilon+E_\beta-E_n)-\mathrm{i}\gamma_n}|n\rangle. \tag{9}$$

The values of γ_n are obtained subject to the normalization condition:

$$\sum_\beta^B \int |\langle n|(\overline{\overline{\beta\varepsilon}})\rangle|^2 \,\mathrm{d}\varepsilon = 1 \tag{10}$$

which means that the probability to find the discrete state $|n\rangle$ in the total number B of the modified continuum channels $|(\overline{\overline{\beta\varepsilon}})\rangle$ (9) is equal to unity. Substituting (9) into (10) and taking into account that in the region nearby $\varepsilon = E_n - E_\beta$ the value of $V_{n\beta}$ depends weakly on energy and therefore can be taken out of the integral (10), yields the following equation for γ_n:

$$\sum_\beta^B \int \frac{V_{n\beta}^2}{(\varepsilon+E_\beta-E_n)^2+\gamma_n^2}\,\mathrm{d}\varepsilon = \sum_\beta^B V_{n\beta}^2 \frac{\pi}{\gamma_n} = 1 \tag{11}$$

$$\gamma_n = \pi \sum_\beta V_{n\beta}^2 . \tag{12}$$

The value

$$\Gamma_n = 2\gamma_n \tag{13}$$

has the meaning of the autoionization width (FWHM) of the state $|n\rangle$ (see also Fano 1961, Combet-Farnoux 1982, Åberg and Howat 1982).

The transition amplitude from the ground state $|0\rangle$ to the $|(\overline{\overline{\beta\varepsilon}})\rangle$ state is obtained from equations (7), (8) and (9):

$$\langle(\overline{\overline{\beta\varepsilon}})|D|0\rangle = \langle\beta\varepsilon|D|0\rangle + \sum_n^N \frac{V_{n\beta}}{(\varepsilon+E_\beta-E_n)+\mathrm{i}\gamma_n}\langle n|D|0\rangle \tag{14}$$

(the sign in the denominator was changed because of the conjugation).

Finally, one should note that equation (14) can be reduced to equations (44)–(46) of Combet-Farnoux (1982) when the case of a single resonance and many continua is under consideration.

2.2. *Two-step model*

The two-step model is an approximation in which the interference of the direct photoionization channel and the ionization through the autoionization of doubly-excited states is not taken into account. The advantage of the model lies in the possibility to determine the following clear physical characteristics of direct photoionization processes and resonance states:

$\sigma_\beta^{\mathrm{d}}(\omega)$, the direct photoionization cross section ($a+c+f$ amplitudes);

σ_n, the excitation cross section of a resonance ($b+d+e$ amplitudes), which is connected with the oscillator strength f_n of the transition from the ground state $|0\rangle$ to the doubly-excited state $|n\rangle$ by the following expression: $\sigma_n = 2\pi^2 \alpha a_0^2 f_n$ (this quantity was calculated in our preceding papers I, II and III);

χ_β^n, the relative partial width or the branching ratio of the $|n\rangle$ state for the decay channel β, which is calculated by the formula:

$$\chi_\beta^n = 2\pi V_{n\beta}^2 / \Gamma_n . \tag{15}$$

This quantity determines what per cent of the total oscillator strength f_n is observed in the decay channel β.

The introduction of the above characteristics allows one to obtain the expression for the photoionization cross section, which is observable in channel $|\beta\varepsilon\rangle$:

$$\tilde{\sigma}_\beta(\omega) = \sigma_\beta^{\mathrm{d}}(\omega) + \sum_n^N L(\varepsilon + E_\beta - E_n, \gamma_n)\sigma_n \chi_\beta^n \tag{16}$$

where $L(\varepsilon + E_\beta - E_n, \gamma_n)$ is a Lorentzian with unity area, and the photon energy ω is connected with the photoelectron energy ε by the following expression

$$\omega + E_0 = \varepsilon + E_\beta . \tag{17}$$

Here E_0 is the atomic ground state energy. The tilde sign in (16) emphasizes that $\tilde{\sigma}_\beta(\omega)$ is an approximate value instead of the exact one, which is

$$\sigma_\beta(\omega) \propto |\langle \overline{\overline{\beta\varepsilon}} | D | 0 \rangle|^2 \tag{18}$$

with the amplitude taken from equation (14). It should be noted that expression (16) can be obtained from equation (18) by use of equation (15) and neglecting the interference effects.

The validity of the two-step model for the description of the photoionization of the Kr atom in the 4s threshold region is an additional problem which is investigated in the present paper.

2.3. *Technique of the calculations*

The aim of this section is to connect the transition amplitudes in scheme (1) with the matrix elements (14) to get the final formulae for numerical calculations. The calculations of the single-electron wavefunctions are similar to those performed in II. Therefore, only the differences in calculations are discussed in the present paper.

2.3.1. Energies and wavefunctions of Kr II ionic states. In scheme (1) [Core] denotes the state of the Kr II ion, characterized by the following wavefunction:

$$|\overline{EJ}\rangle = \sum_{\alpha\bar{L}\bar{S}} \langle \alpha\bar{L}\bar{S}\bar{J}|\overline{EJ}\rangle \alpha\bar{L}\bar{S}\bar{J}\rangle \tag{19}$$

where $\bar{E}$ is the energy of the residual ion with total momentum $\bar{J}$, $\bar{L}$ and $\bar{S}$ are orbital and spin momenta of the basis state, respectively, and α denotes the remaining quantum numbers of the basis state. In equation (19) and the following the energy $\bar{E}$ corresponds to the threshold energy (or ionization potential) E_β in equation (5). The details of the calculations of eigenenergies $\bar{E}$ and eigenfunctions $|\overline{EJ}\rangle$ in the intermediate-coupling scheme taking into account many-electron correlations were described in II. The only point we would like to stress here is connected with the basis states $|\alpha\overline{LSJ}\rangle = |4p^4(L_0S_0)(\varepsilon s/\varepsilon d)\overline{LSJ}\rangle$. It is known (Smid and Hansen 1983, II) that these states have a large influence on the values of eigenenergies $\bar{E}$ and numerical coefficients $\langle\alpha\overline{LSJ}|\overline{EJ}\rangle$ in eigenfunctions $|\overline{EJ}\rangle$. Therefore they were included in (19) but were not taken into account in the calculations of the transition amplitudes in scheme (1).

In column c of table 1 the $\bar{E}$ values for several channels are presented and compared with the measured ones (Sugar and Musgrove 1991). The table demonstrates that the accuracy of the calculations is equal to ~0.05 meV. In column b of the same table the largest squared coefficients $\langle\alpha\overline{LSJ}|\overline{EJ}\rangle^2 \times 100\%$ of the eigenfunctions $|\overline{EJ}\rangle$ are presented. It is obvious from the data that the assignments of the levels in the tables of Sugar and Musgrove (1991) indicate only the genealogy of the ionic states. The branching ratios, χ^n_β, calculated using equation (15) are also presented in table 1 and will be discussed in section 3.

2.3.2. Energies and wavefunctions of doubly-excited states. The notation [Core]*n*p of a doubly-excited state in scheme (1) corresponds to the discrete state $|n\rangle$ in equation (14). In the present paper the doubly-excited states with p symmetry only of an outer electron were included in the calculations, because the oscillator strengths f_n are large in those states (I, II). More specifically, the set of doubly-excited states is restricted to those states with 5p and 6p electrons which have large oscillator strengths. This set is exactly the same as in our previous calculations (table 7 in II).

The wavefunctions of [Core]*n*p doubly-excited states have been presented in the form:

$$|EJ\rangle = \sum_{\bar{E}\bar{J}nj} \langle \overline{EJ}npjJ|EJ\rangle |\overline{EJ}npjJ\rangle \tag{20}$$

where the numerical coefficients $\langle\overline{EJ}npjJ|EJ\rangle$ of the eigenfunctions were obtained by solving the secular equation of 54th order, according to the above-described limitations on the doubly-excited state basis set:

$$\det\|\langle\overline{EJ}npjJ|H^{ee} - H^{ee}_{HF}|\bar{E}'\bar{J}'npj'J\rangle - E\delta_{E,E'}\delta_{J,J'}\delta_{n,n'}\delta_{j,j'}\| = 0. \tag{21}$$

In equations (20) and (21) J is the total momentum of doubly-excited states, equal to unity because of the dipole selection rules, j is the total momentum of the np electron, and $|\overline{EJ}\rangle$ is the eigenfunction (19) of the Kr II ion. H^{ee} and H^{ee}_{HF} are the exact and the average Hartree–Fock (HF) Hamiltonians describing the Coulomb interaction. In the numerical calculations each wavefunction $|\overline{EJ}npjJ\rangle$ was expanded with respect to the

Table 1. Characteristics of satellite states and branching ratios for the decay of doubly-excited states.

Characteristics of satellite states				Characteristics of doubly-excited states													
Assignment		$\bar{E}$ (eV)		No[e]	9	10	11	12	13	14	15	16	17	18	19	20	22
[a]	[b]	[c]	[d]	E (eV)[f]	28.52	28.98	29.13	29.24	29.32	29.44	29.51	29.63	29.86	30.02	30.17	30.43	30.65
				$f_{EJ}/10^{-3}$ [g]	1.26	0.03	0.60	1.69	6.57	2.27	1.27	3.28	7.03	0.78	0.27	0.88	0.83
[4s $^2S_{1/2}$	64%]	27.54	−0.03		48[h]	11	6	0	12	22	1	8	0	3	0	0	0
+[(^{3}P)5s $^4P_{1/2}$	93%]	28.52	0.06		0	1	12	0	1	4	1	21	0	3	2	8	29
+[(^{3}P)5s $^4P_{3/2}$	64%]	28.24	0.03		12	5	2	12	3	2	5	5	0	21	1	0	0
+[(^{3}P)5s $^4P_{5/2}$	96%]	27.98	0.01		3	25	18	49	25	3	19	0	0	8	0	0	5
+[(^{3}P)5s $^2P_{1/2}$	91%]	28.94	0.06			0	5	0	4	4	1	0	0	6	0	5	0
+[(^{3}P)5s $^2P_{3/2}$	63%]	28.63	0.06			0	15	0	4	1	4	9	1	8	1	1	1
+[(^{3}P)4d $^4D_{1/2}$	92%]	29.13	−0.03			0	0	0	0	5	0	0	0	2	0	0	0
+[(^{3}P)4d $^4D_{3/2}$	91%]	29.05	−0.05			0	1	5	0	5	4	1	0	1	1	0	1
+[(^{3}P)4d $^4D_{5/2}$	92%]	28.98	−0.05			0	10	12	3	3	11	6	1	3	5	1	3
[(^{3}P)4d $^4D_{7/2}$	94%]	28.94	−0.04			41	0	13	2	16	17	14	1	6	0	0	2
+[(^{1}D)5s $^2D_{3/2}$	82%]	29.82	0.00										27	12	1	20	3
+[(^{1}D)5s $^2D_{5/2}$	91%]	29.84	0.01										52	5	25	56	23
[(^{3}P)4d $^4F_{3/2}$	97%]	30.17	0.01											0	0	0	4
[(^{3}P)4d $^4F_{5/2}$	94%]	30.07	0.01											0	3	1	4
[(^{3}P)4d $^4F_{7/2}$	86%]	29.88	−0.02											8	3	0	0
[(^{3}P)4d $^4F_{9/2}$	96%]	29.64	−0.02											1	3	0	0

[a] '+' sign denotes the satellite states which are included in $\sigma_{sat}(\omega)$ (equation (37)).
[b] Percentage of the basis state, $|\alpha\overline{LSJ}\rangle$, in the Kr II ionic state $|\overline{EJ}\rangle$ (19).
[c] $\bar{E}$ calculated energy of the Kr II ionic state $|\overline{EJ}\rangle$ (19).
[d] $\Delta\bar{E}=\bar{E}_{exp}$ (Sugar and Musgrove 1991) $-\bar{E}$.
[e] The numerical designations of the doubly-excited states according to table 3.
[f] Calculated energy E of doubly-excited state $|EJ\rangle$ (20).
[g] Oscillator strength f_{EJ} (see equation (36)).
[h] Branching ratio $\chi_{\overline{EJ}}^{EJ}$ (35) (in per cent) of the doubly-excited state $|EJ\rangle$ for the decay channel with the final ionic state $|\overline{EJ}\rangle$.

LS-coupling basis vectors $|\alpha\overline{LS}np_sLSJ\rangle$ with a definite electronic configuration by

$$|\overline{EJ}np_jJ\rangle = \sum_{\alpha\overline{LS}} \langle \alpha\overline{LSJ}|\overline{EJ}\rangle \sum_{LS} [(2L+1)(2S+1)(2\bar{J}+1)(2j+1)]^{1/2} \times \begin{Bmatrix} \bar{L} & \bar{S} & \bar{J} \\ 1 & s & j \\ L & S & J \end{Bmatrix} |\alpha\overline{LS}np_sLSJ\rangle. \tag{22}$$

In the calculations of the matrix elements

$$\langle \alpha\overline{LS}np_sLSJ|H^{ee} - H^{ee}_{HF}|\alpha'\bar{L}'\bar{S}'n'p_sL'S'J\rangle \tag{23}$$

arising after the substitution of (22) into (21), each Slater integral was reduced by a factor 1.26 because of the correlational Coulomb interaction decrease, which was described and calculated in II.

The ionization potentials IP(np) of the np electrons in the configuration K, which appear in the diagonal matrix elements (23), were calculated in the present paper by taking into account the correlation effects using the formula:

$$\Delta IP_K(np) = IP_K(np) - IP_K^{HF}(np) = C(K) - C(K+np). \tag{24}$$

Here $IP_K(np)$ and $IP_K^{HF}(np)$ are the exact and the HF ionization potentials of an np electron in the configuration K, respectively, $C(K)$ and $C(K+np)$ are the total correlation energies of configuration K (without an np electron) and $K+np$ (with an np electron), respectively. The technique of the correlation correction calculations was described in our earlier papers I and II. The present calculations differ from the previous ones (II) in two particular points. Firstly, in this paper the set of virtual states was extended with respect to the calculations in II by adding $\{i\}$-channels ($l=6$) and by increasing the integration interval over continuous intermediate states from 0 to 400 Ryd to 0 to 1500 Ryd. Secondly, the different sets of intermediate virtual atomic orbitals (AO), obtained in self-consistent fields of the ($K-4p$) and the ($K+np-4p$) configurations, were involved in $C(K)$ and $C(K+np)$ calculations, respectively. The results of these calculations are presented in table 2. One can see that the extension of virtual AO space and taking into account the rearrangement effects lead to changing the IP(np) values by a few tenths of an eV.

Table 2. Ionization potentials (in eV) of np electrons calculated in different configurations.

	$IP_K(5p)$			$IP_K(6p)$		
K	HF[a]	Corr.[b]	Corr.[c]	HF[a]	Corr.[b]	Corr.[c]
$4s^{-1}$ np	2.37	2.79	2.58	1.13	1.42	1.19
$4p^{-2}4d$ np	2.67	3.25	2.83	1.20	1.52	1.28
5d np	4.40	4.72	4.61	1.57	1.75	1.63
6d np	5.43	5.61	5.64	2.00	2.10	2.06
7d np	5.98	6.08	6.19	2.66	2.71	2.72
8d np	6.32	6.37	6.53	2.97	3.00	3.03
5s np	2.99	3.37	3.24	1.25	1.44	1.28
6s np	4.27	4.46	4.48	1.63	1.73	1.69

[a] HF approximation.

[b] IP_K, corrected according to equation (24).

[c] IP_K from the work of Sukhorukov *et al* (1994).

2.3.3. Amplitudes and probabilities of non-radiative transitions. The matrix element $V_{n\beta}$ in equation (14) corresponds to the transition amplitude h in scheme (1) and is responsible for the autoionization decay of doubly-excited states. The wavefunction of the doubly-excited state $|EJ\rangle$ was expressed by equation (20), and the wavefunction $|\beta\varepsilon\rangle$ of the continuous state was taken in the following form:

$$|\beta\varepsilon\rangle = |\overline{EJ}\varepsilon ljJ\rangle. \tag{25}$$

In the present paper $\varepsilon lj \in \{\varepsilon p_{1/2}, \varepsilon p_{3/2}, \varepsilon f_{5/2}, \varepsilon f_{7/2}\}$. It is clear that the wavefunctions (25) differ from (22) only by replacing np by εl. Therefore, the calculations of the matrix elements

$$V_{n\beta} = \langle \overline{EJ}\varepsilon ljJ|H^{ee}|EJ\rangle \tag{26}$$

were performed by using a formula similar to equation (23).

The contribution of the autoionization of doubly-excited states to the total width of a resonance state Γ_n (equation (13)) was determined by the formula:

$$\Gamma_{\text{Auto}}(EJ) = 2\pi \sum_{\overline{EJ}lj} |\langle \overline{EJ}\varepsilon ljJ|H^{ee}|EJ\rangle|^2. \tag{27}$$

This autoionization width is connected with the following transitions h in scheme (1): $4s^24p^4(ns/nd)np \rightarrow 4s^14p^6\varepsilon p$ or $4s^24p^4(ns/nd)np \rightarrow 4s^24p^4(ns/nd)\varepsilon l$. In equation (27) the summation over all channels with the threshold energies $\bar{E}$ less than the energy E of a resonance state was performed.

The formula for the probability of Auger decay of doubly-excited states $|EJ\rangle$ (the transition g in scheme (1)) is very similar to (27):

$$\Gamma_{\text{Auger}}(EJ) = 2\pi \sum_{\bar{J}jl} |\langle 4p^5\bar{J}\varepsilon lj|H^{ee}|EJ\rangle|^2. \tag{28}$$

In the calculations performed, the expansion of the $|4p^5\bar{J}\varepsilon ljJ\rangle$ wavefunction with respect to the LS-coupling basis states was carried out, and $\{\varepsilon lj\} \in \{\varepsilon s_{1/2}, \varepsilon d_{3/2}, \varepsilon d_{5/2}\}$. The total width of a resonance state $|EJ\rangle$ was determined by the formula:

$$\Gamma(EJ) = \Gamma_{\text{Auto}}(EJ) + \Gamma_{\text{Auger}}(EJ). \tag{29}$$

2.3.4. Amplitudes of radiative transitions and photoionization cross sections. Using equation (20) for the $|n\rangle$ state, equation (26) for the $V_{n\beta}$ matrix element, equation (29) for the $2\gamma_n$ width, and equation (25) for the $|\beta\varepsilon\rangle$ state, one can obtain the expression for the photoionization cross section, which is presented in the velocity form:

$$\sigma_{\overline{EJ}}(\omega) = \frac{4}{3}\frac{\pi^2\alpha a_0^2}{\omega}\sum_{lj}\left|\langle \overline{EJ}\varepsilon ljJ|D|0\rangle + \sum_{EJ}\frac{\langle \overline{EJ}\varepsilon ljJ|H^{ee}|EJ\rangle\langle EJ|D|0\rangle}{(\varepsilon+\bar{E}-E)+i\Gamma(EJ)/2}\right|^2 \tag{30}$$

where

$$\omega = \varepsilon + E \tag{31}$$

$J=1$ because of dipole selection rules, and $l_j = \{p_{1/2}, p_{3/2}, f_{5/2}, f_{7/2}\}$. According to scheme (1) and the calculation technique of Amusia and Cherepkov (1975), I and II, the matrix elements of the transition operator D contain the Coulomb and the dipole parts. The technique of transition matrix element calculations is similar to the one presented in II and will not be described here. The velocity form seems to be preferable in the numerical calculations, though, as was mentioned in I and II, the cross section

values in the near 4s threshold region, calculated both in length σ_r and velocity σ_v forms, differ from each other by less than 5%. Our preference for the velocity form in the transition matrix element calculations is based on the following experience. In most cases, σ_v calculated in second-order PT agrees closely with σ_v calculated with higher-order PT corrections. In the calculations in the length form, however, this agreement is less close.

The formulae which were used in the present calculations within the two-step model are the following:

$$\tilde{\sigma}_{\overline{EJ}}(\omega)=\sigma^{d}_{\overline{EJ}}(\omega)+\sum_{EJ} L(\omega-E,\Gamma(EJ)/2)\sigma_{EJ}\chi^{EJ}_{\overline{EJ}} \tag{32}$$

$$\sigma^{d}_{\overline{EJ}}(\omega)=\frac{4}{3}\frac{\pi^2\alpha a_0^2}{\omega}\sum_{lj}|\langle\overline{EJ}\varepsilon ljJ|D|0\rangle|^2 \tag{33}$$

$$\sigma_{EJ}=\frac{4}{3}\frac{\pi^2\alpha a_0^2}{\omega}|\langle EJ|D|0\rangle|^2 \tag{34}$$

$$\chi^{EJ}_{\overline{EJ}}=\frac{2\pi\,\Sigma_{lj}|\langle\overline{EJ}\varepsilon ljJ|H^{ee}|EJ\rangle|^2}{\Gamma(EJ)} \tag{35}$$

and the oscillator strengths f_{EJ} of the transitions into doubly-excited states $|EJ\rangle$ are connected with the σ_{EJ} values by the expression:

$$\sigma_{EJ}=2\pi^2\alpha a_0^2 f_{EJ}. \tag{36}$$

3. Results and discussion

The calculated 4s photoionization cross section and the cross sections for the production of some Kr II satellite states are presented and compared with our experimental values in figures 1–4. The calculations have been performed taking into account the interference of various photoionization channels by using equation (30). The quantities which are necessary for the calculations of the spectra and for the assignments of the resonances in the spectra are collected in tables 1 and 3. The theoretical widths $\Gamma_{Auger}(EJ)$, $\Gamma_{Auto}(EJ)$, $\Gamma(EJ)$ and the energies E of doubly-excited states $|EJ\rangle$ which enter equation (30) are presented in table 3. The energies $\bar{E}$ of ionic states $|\overline{EJ}\rangle$ are presented in table 1.

The strongest resonances in the theoretical spectra were assigned. A list of assignments is presented in table 3. The numbering of the resonances in table 1 and figures 1–4 is consistent with table 3. To make these assignments the two-step model was applied and the following characteristics of the resonances were used (table 1): the oscillator strengths f_{EJ} of the transitions to doubly-excited states (see equation (36)), the energies E of doubly-excited states and the branching ratios $\chi^{EJ}_{\overline{EJ}}$ (35). The genealogy of each doubly-excited state listed in table 3 is characterized by the largest squared coefficient $\langle\overline{EJ}npjJ|EJ\rangle$ (column a) of the basis state in equation (20) and this basis state is used to assign the $|EJ\rangle$ state. The assignments of the respective Kr II ionic states $|EJ\rangle$ are given in accordance with Sugar and Musgrove (1991) and II, and the genealogical characteristics of these ionic states are also presented in column b of table 3 (as well as table 1). As one can see from table 3, the $|\overline{EJ}npjJ\rangle$ basis states are considerably mixed in most cases and, therefore, the proposed assignments of doubly-excited states are to some extent arbitrary. The summed values of branching ratios for

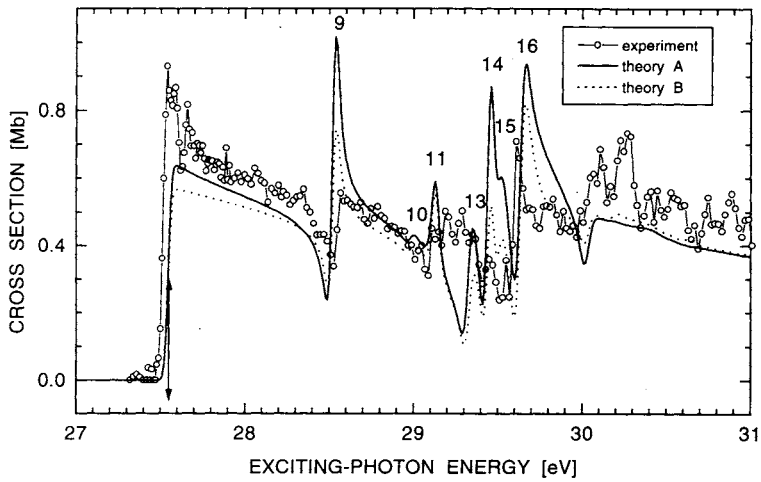

Figure 1. Photoionization cross sections for the Kr II 4s state measured and calculated with (A) and without (B) taking into account the resonances below the 4s threshold. The experimental values have been taken from III. The calculated ionization threshold of the level has been marked by the double arrow line. The numbering of the resonances is consistent with the one presented in tables 1 and 3.

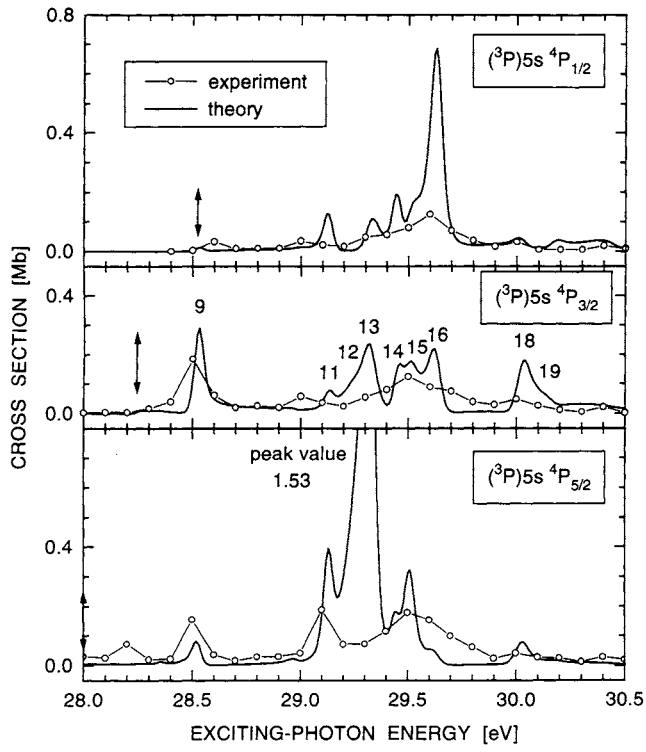

Figure 2. Experimental and theoretical photoionization cross sections for the Kr II $(^3P)5s\ ^4P_J$ satellite states. Experimental data from I and II (see text). The calculated ionization threshold of the level has been marked by the double arrow line. The numbering of the resonances is consistent with the one presented in tables 1 and 3.

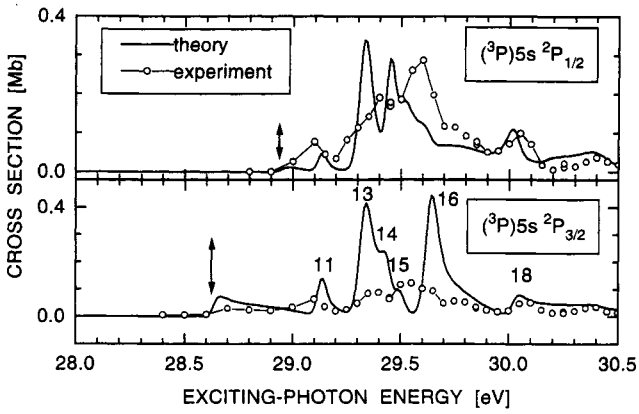

Figure 3. Experimental and theoretical photoionization cross sections for the Kr II $(^3P)5s\ ^2P_J$ satellite states. Experimental data from I and II (see text). The calculated ionization threshold of the level has been marked by the double arrow line. The numbering of the resonances is consistent with the one presented in tables 1 and 3.

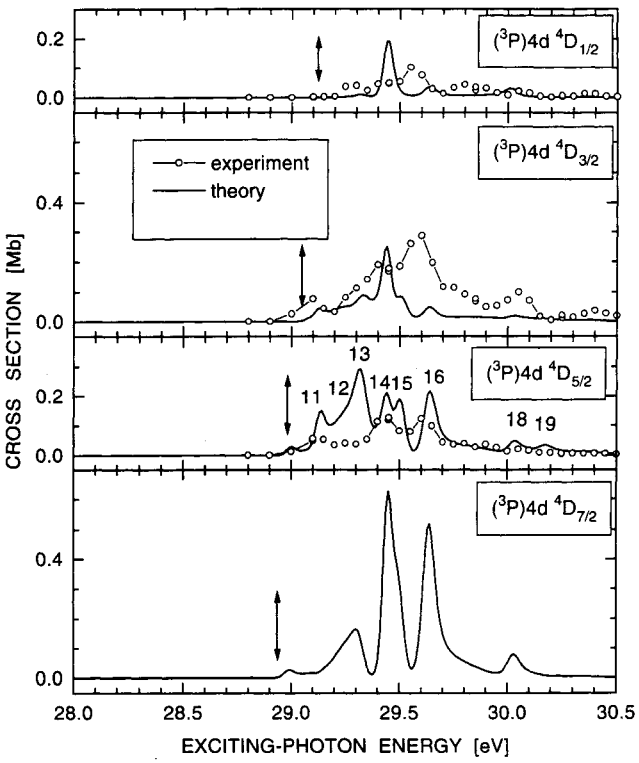

Figure 4. Experimental and theoretical photoionization cross sections for the Kr II $(^3P)4d\ ^4D_J$ satellite states. Experimental data from I and II (see text). The calculated ionization threshold of the level has been marked by the double arrow line. The numbering of the resonances is consistent with the one presented in tables 1 and 3.

Table 3. Characteristics of doubly-excited states in the two-step model.

No	Assignment [a]		[b]	Energy E (eV)	Oscill. strength $f_{EJ}/10^{-3}$	Widths (meV) Auger	Auto	Total $\Gamma(EJ)$	$\bar{\chi}_{EJ}^{\text{sat}}$ [c] (%)
1	50%	$[(^1D)5s\ ^2D_{5/2}\ 5p_{3/2}$	91%]	27.06	1.98	10.10	0.00	10.10	0
2	86%	$[(^3P)5s\ ^2P_{3/2}\ 6p_{1/2}$	63%]	27.17	0.01	0.56	0.00	0.56	0
3	75%	$[(^3P)5s\ ^2P_{3/2}\ 6p_{3/2}$	63%]	27.27	0.90	3.95	0.00	3.95	0
4	74%	$[(^3P)5s\ ^2P_{1/2}\ 6p_{1/2}$	91%]	27.52	0.01	1.00	0.00	1.00	0
5	73%	$[(^3P)5s\ ^2P_{1/2}\ 6p_{3/2}$	91%]	27.52	0.09	1.30	0.00	1.30	0
6	58%	$[(^1D)5s\ ^2D_{3/2}\ 6p_{3/2}$	82%]	28.31	0.00	2.89	27.22	30.10	88
7	55%	$[(^1D)5s\ ^2D_{3/2}\ 6p_{1/2}$	82%]	28.35	0.01	0.78	1.75	2.54	69
8	52%	$[(^1S)5s\ ^2S_{1/2}\ 5p_{1/2}$	85%]	28.44	0.00	6.51	1.07	7.58	13
9	60%	$[(^1D)5s\ ^2D_{5/2}\ 6p_{3/2}$	91%]	28.52	1.26	6.69	12.29	18.98	16
10	36%	$[(^1D)4d\ ^2P_{3/2}\ 5p_{1/2}$	43%]	28.98	0.03	3.13	19.11	22.24	74
11	35%	$[(^1S)5s\ ^2S_{1/2}\ 5p_{3/2}$	85%]	29.13	0.60	5.25	14.07	19.31	66
12	34%	$[(^1D)4d\ ^2P_{3/2}\ 5p_{3/2}$	43%]	29.24	1.69	11.86	148.77	160.63	92
13	28%	$[(^1D)4d\ ^2D_{5/2}\ 5p_{3/2}$	45%]	29.32	6.57	19.99	27.63	47.62	45
14	44%	$[(^1D)4d\ ^2D_{3/2}\ 5p_{3/2}$	48%]	29.44	2.27	5.67	13.77	19.44	48
15	45%	$[(^1D)4d\ ^2P_{1/2}\ 5p_{3/2}$	46%]	29.51	1.27	10.93	23.81	34.74	66
16	39%	$[(^1D)4d\ ^2D_{3/2}\ 5p_{1/2}$	48%]	29.63	3.28	14.06	30.26	44.32	60
17	26%	$[(^1D)4d\ ^2P_{1/2}\ 5p_{1/2}$	46%]	29.86	7.03	39.90	274.26	314.15	87
18	80%	$[(^3P)5d\ ^4F_{5/2}\ 5p_{3/2}$	42%]	30.02	0.78	3.77	46.90	50.67	89
19	52%	$[(^1D)4d\ ^2S_{1/2}\ 5p_{1/2}$	47%]	30.17	0.27	24.39	25.82	50.21	51
20	39%	$[(^3P)5d\ ^2D_{5/2}\ 5p_{3/2}$	54%]	30.43	0.88	1.59	175.55	177.14	99
21	53%	$[(^1S)5s\ ^2S_{1/2}\ 6p_{1/2}$	85%]	30.55	0.01	2.01	21.29	23.30	91
22	42%	$[(^1S)5s\ ^2S_{1/2}\ 6p_{3/2}$	85%]	30.65	0.83	1.57	21.15	22.72	93

[a] Percentage of the basis state, $|\alpha\overline{LSJ}npjJ\rangle$, in the doubly-excited Kr I atomic state $|EJ\rangle$ (20);
[b] Percentage of basis state, $|\alpha\overline{LSJ}\rangle$, in the Kr II ionic state $|\overline{EJ}\rangle$ (19);
[c] The total probability to observe the $|EJ\rangle$ doubly-excited state in all final satellite states (equation (39)).

doubly-excited states, which are presented in the last column in table 3 will be discussed in section 3.3.

For the convenient comparison of experimental and theoretical spectra, the calculated cross sections were convoluted with a Gaussian apparatus profile. A width of 40 meV (FWHM) was reached in the measurements of the 4s-photoionization cross section published in III. The FWHM in the measurements of the cross sections for the satellite states (I) was equal to $\approx$150 meV.

We have to point out that, due to an unfortunate mistake in the absolute evaluation of the population cross sections of satellite states after photoionization, the published satellite state cross sections in I and II are too large by a factor of 2.25 and have to be divided by this constant factor. The published absolute 4s photoionization cross sections of the Kr atom remain unchanged.

3.1. 4s-main line

The comparison of the measured 4s photoionization cross section with the calculated one is presented in figure 1. One can see that the theory reproduces many features of the experimental spectrum. In the region from threshold up to 29 eV, e.g., which contains a single resonance no 9 only at 28.5 eV, the agreement is impressive. Between 29 eV and 30 eV, the existence of many resonances is reproduced by theory. The cross section averaged over the resonances is also in good agreement with the measurements, whereas

the details of these resonances are still incomplete. One can suppose several possible ways to improve the calculations. Firstly, we expect the additional fine structure in the calculated spectrum in the region from 29 to 30 eV to appear after the inclusion in (20) of [Core]np ($n=5, 6$) states with small oscillator strengths, and [Core]np ($n>6$) and [Core]nf doubly-excited states, lying in this energy range. Secondly, the influence of np electrons on the wavefunctions of the [Core] electrons has to be taken into account.

It is necessary to point out that the autoionization decay amplitudes of the doubly-excited states, which were considered in the present paper, could be essentially changed after taking into account, as described above, additional states for the following reasons. A separate investigation showed that the amplitudes of the autoionization decay of [Core]nl doubly-excited states decrease with increasing n and l values much less than the excitation amplitudes. This is caused by the fact that the excitation of [Core]nl states is allowed only through the channel with the $^1P_1$ angular momenta, while the decay can proceed through the $^1P_1$, $^3P_1$, and $^3D_1$ channels.

It is important to note also that in the calculations of the 4s photoionization cross section the doubly-excited states with energies less than the 4s threshold value also play a significant role. Including these states in the calculations leads to a change of the excitation and decay amplitudes of the resonances and to a change in the cross section of the direct photoionization at energies close to threshold. This is demonstrated in figure 1, where the results of calculations with and without those basis states (22), which mainly determine the doubly-excited states (20) below threshold (i.e. states nos 1–5 in table 2), are presented.

3.2. Cross sections for the production of the satellite states

The calculated cross sections for the population of some satellite states are compared in figures 1–4 with our previously measured values (I and II, with scaling factor 1/2.25 as described above). The upper energy limit in the calculations was restricted to the value 30.5 eV. This is caused by the fact that additional photoionization channels, connected with the population of odd core states, open up if $\omega > 30.5$ eV (e.g. $E(4p^4(^4P)5p\ ^4P_{5/2} = 30.60$ eV (Sugar and Musgrove 1991)). This leads to additional population channels of even Kr II states via fluorescence cascades. These cascades have not been included in the calculations. The population cross section for the $(^3P)4d\ ^4D_{7/2}$ satellite state could not be observed in the PIFS measurements since transitions from states with $J=\frac{7}{2}$ to the final states with $J=\frac{1}{2}$ or $J=\frac{3}{2}$ are forbidden by the dipole selection rules.

From figure 2 one can see that similar to the main-line calculations in cases of the separate resonances at 28.5 eV the agreements between the theory and experiment are good. As was mentioned above, a reliable comparison of the details of theoretical cross sections with measured ones in the region of 29 to 30 eV would become possible after improvement of the calculations by including of [Core]np ($n>6$) and [Core]nf doubly-excited states in the basis set. Nevertheless, within the present calculations' approach there is satisfactory agreement in the basic elements of the theoretical and experimental $\sigma_{\overline{EJ}}(\omega)$ spectra for many levels.

To test the accuracy of the calculated total value of the cross sections for the population of doubly-excited states, the measured cross sections of the satellite levels

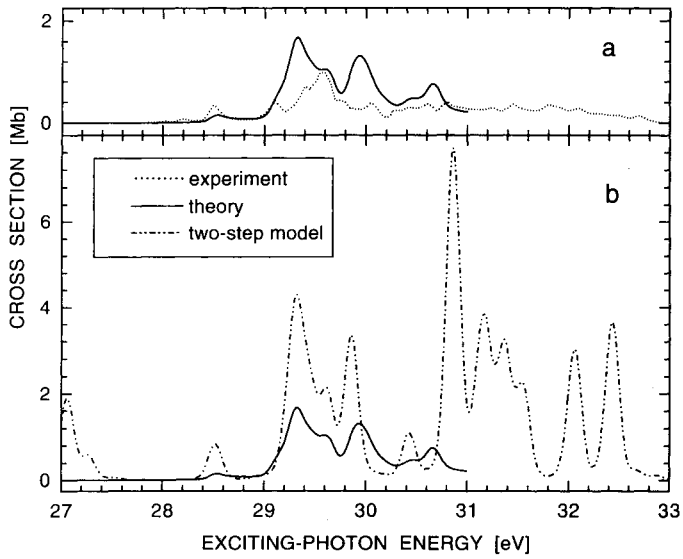

Figure 5. Comparison of the measured and calculated total cross section, $\sigma_{sat}(\omega)$, for the population of all Kr II satellite states considered. (*a*) experiment (dotted curve) and calculations by equation (37) (full curve); (*b*) calculations by equation (37) (full curve) and in a two-step model (chain curve) including the doubly-excited states with energies higher than 30.5 eV (see section 3.3).

shown in figures 2–4 were summed. The results of this summation are presented in figure 5(*a*). The calculated values of $\sigma_{sat}(\omega)$,

$$\sigma_{sat}(\omega) = \sum_{\overline{EJ}} \sigma_{\overline{EJ}}(\omega) \tag{37}$$

were also obtained by summation of partial satellite cross sections $\sigma_{\overline{EJ}}(\omega)$ (30) of levels marked by a '+' sign in table 1. The calculated $\sigma_{sat}(\omega)$ is presented in figure 5(*a*) after convolution with a Gaussian of 150 meV FWHM.

The comparison between the measured and the calculated values of $\sigma_{sat}(\omega)$ shows that these theoretical values are somewhat larger than the measured ones. This fact can be connected with the necessity to incorporate the rearrangement of electron shells in the cross section calculations.

3.2.1. Two-step model. To check the validity of the two-step model discussed above for the description of the cross sections for the photoionization of the 4s state and satellite states, the values $\tilde{\sigma}_{\overline{EJ}}(\omega)$ were calculated using equation (32). The results of the calculations are compared in figure 6 with accurate values $\sigma_{\overline{EJ}}(\omega)$, obtained by equation (30), for the three levels. The direct photoionization cross sections $\sigma^{d}_{\overline{EJ}}(\omega)$, calculated by equation (33), are also presented.

One can see that in case of large $\sigma^{d}_{\overline{EJ}}(\omega)$ values (4s state), the two-step model gives only a rough estimate of the influence of the resonance states on the cross section. In the case of intermediate $\sigma^{d}_{\overline{EJ}}(\omega)$ values ($(^3P)5s\ ^2P_{3/2}$ state), the two-step model is rather good but cannot describe all details of the fine structure. Finally, if $\sigma^{d}_{\overline{EJ}}(\omega)$ is small ($(^3P)5s\ ^3P_{1/2}$ state), the two-step model is valid and can be used for quantitative calculations of the cross sections.

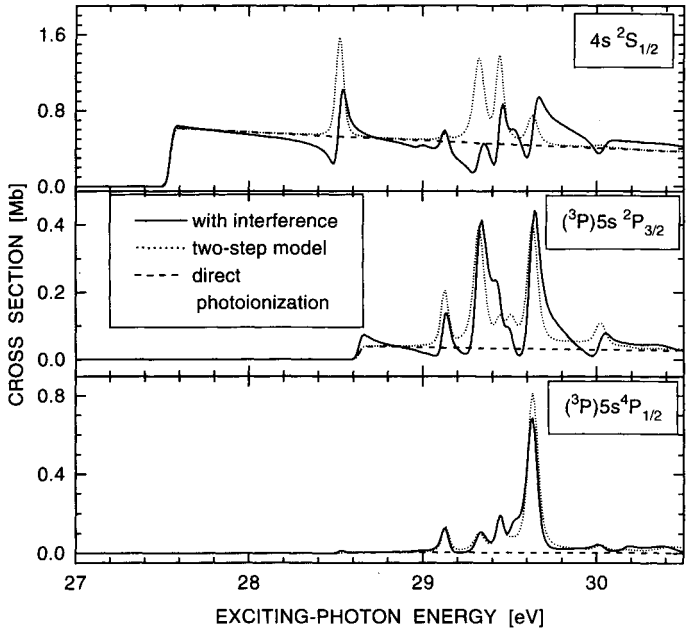

Figure 6. Theoretical photoionization cross sections for selected (see section 3.3) Kr II states, calculated with (full curve) and without (dotted curve) taking into account the interference of the channels of direct photoionization and autoionization of doubly-excited state.

The main advantage of the two-step model lies in the possibility of analysing the main spectral features by only calculating the oscillator strengths, f_{EJ} (equation (36)), of the transitions to the doubly-excited states. For example, the comparison of the total oscillator strength for the transitions to doubly-excited states in the ω region from 28 to 30 eV calculated in the present work and in II, demonstrates that the total oscillator strength in this region is reduced by a factor of 1.52 in the present work. This value is obtained if one adds the f_{EJ} values of the doubly-excited states nos 6–17 from table 3 and divides the result by the sum of the f_{EJ} values for the same states from table 7 in II. Furthermore, in present accurate calculations of an interaction of $|\overline{EJ}\rangle$ core electrons with np electrons in the doubly-excited states the decrease of f_{EJ} described above is accompanied by an increase of f_{EJ} in the ω region of 30 to 33 eV. The possible manifestation of this oscillator strength redistribution in the experiment will be discussed at the end of this section.

For the isolated resonance no 9 it is possible to make a simple illustration of the oscillator strength redistribution. This possibility is based on the fact that the description of interference effects in this resonance is determined by the interaction between two basis states only, namely $|B1\rangle = |(^1S)5s\ ^2S_{1/2}\ 5p_{1/2}\rangle$ and $|B2\rangle = |(^1S)5s\ ^2S_{1/2}\ 5p_{3/2}\rangle$. The real (Re) and the imaginary (Im) parts of the transition amplitudes to the $|B1\rangle$ and $|B2\rangle$ basis states, calculated according to scheme (1), are presented in table 4. The eigenfunctions $|B1'\rangle$ and $|B2'\rangle$ and eigenenergies of the states obtained after the diagonalization of the second-order matrix (21) are presented at the bottom of table 4 together with the transition amplitudes and oscillator strengths for the $|B1'\rangle$ and $|B2'\rangle$ states.

One can see that after the interference of the $|B1\rangle$ and $|B2\rangle$ basis states the oscillator strength of a transition to the mixed state $|B1'\rangle$ with the energy $E = 28.43$ eV is reduced

Table 4. Illustration of oscillator strength redistribution.

Basis states and eigenfunctions	E (eV)	Transition amplitudes[a] Re	Im	$f_{EJ}/10^{-3}$
$\|B1\rangle = 4p^4(^1S)5s\ ^2S_{1/2}\ 5p_{1/2}$	28.77	−0.0515	−0.0089	2.73
$\|B2\rangle = 4p^4(^1S)5s\ ^2S_{1/2}\ 5p_{3/2}$	29.09	−0.0695	−0.0136	5.01
$\|B1'\rangle = 0.8128\|B1\rangle - 0.5825\|B2\rangle$	28.43	−0.0014	0.0007	0.002
$\|B2'\rangle = 0.5825\|B1\rangle + 0.8128\|B2\rangle$	29.43	−0.0865	−0.0162	7.74

[a] The transition amplitudes are scaled so that $\mathrm{Re}^2 + \mathrm{Im}^2 = f$.

by a factor of $2.73/0.002 \approx 1400$ and becomes negligibly small. Therefore, the resonance which is observed with an energy of ~28.5 eV should be assigned to the $(^1D)5s\ ^2D_{5/2}\ 6p_{3/2}$ doubly-excited state and not to the $(^1S)5s\ ^2S_{1/2}\ 5p_{1/2}$ state as it was assumed in I and II. It should be noted, however, that the fraction of the $(^1D)5s\ ^2D_{5/2}\ 6p_{3/2}$ basis state in the $|EJ\rangle$ doubly-excited state with an energy of 28.52 eV is equal to 54%.

It was discussed above and illustrated in figure 6 that the two-step model describes the cross sections for the satellite states quite well. This fact allows one to apply the model to determine $\tilde{\sigma}_{\mathrm{sat}}(\omega)$, the estimation of the total $\sigma_{\mathrm{sat}}(\omega)$ (37), by the summation of $\tilde{\sigma}_{\overline{EJ}}(\omega)$ values (32) over $\overline{EJ}$ values:

$$\tilde{\sigma}_{\mathrm{sat}}(\omega) = \sum_{\overline{EJ}} \sigma^{\mathrm{d}}_{\overline{EJ}}(\omega) + \sum_{EJ} L(\omega - E, \Gamma(EJ)/2)\sigma_{EJ}\bar{\chi}^{\mathrm{sat}}_{EJ} \tag{38}$$

where the summed value of branching ratios for doubly-excited states $|EJ\rangle$ is determined by

$$\bar{\chi}^{\mathrm{sat}}_{EJ} = \sum_{\overline{EJ}}^{\mathrm{sat}} \chi^{EJ}_{\overline{EJ}}. \tag{39}$$

The quantity $\bar{\chi}^{\mathrm{sat}}_{EJ}$ describes the total probability to observe the $|EJ\rangle$ doubly-excited state in all final satellite states (the 4s main state is excluded). These values are presented in table 2. One can see that they become approximately equal to 90% when the energy E increases above the 4s threshold value. If one takes into account that the direct photoionization cross section for the satellite states is relatively small, then equation (38) can be approximated by the following expression:

$$\tilde{\sigma}_{\mathrm{sat}}(\omega) = \sum_{EJ} L(\omega - E, \Gamma(EJ)/2)\sigma_{EJ}. \tag{40}$$

If one also takes into account that equation (40) was obtained under certain approximations and that the apparatus profile for most of the measured satellite state cross section spectra is much wider than the natural width, the $\Gamma(EJ)$ value can be assumed constant for all $|EJ\rangle$ states. Consequently, $\sigma_{\mathrm{sat}}(\omega)$ can be evaluated according to equation (40) by only calculating the oscillator strength of the transitions to doubly-excited states.

The results of $\sigma_{\mathrm{sat}}(\omega)$ calculations, performed with equation (40) and $\Gamma(EJ) = 20$ meV and following the convolution with a Gaussian apparatus profile with 150 meV FWHM, are presented in figure 5(*b*). The theoretical values of $\sigma_{\mathrm{sat}}(\omega)$, obtained by equations (37) and (30), are also presented. The comparison shows that in the energy region from 28 to 30 eV, equation (40) gives quite a good estimation of $\sigma_{\mathrm{sat}}(\omega)$ values. This fact allows one to use the approximate $\tilde{\sigma}_{\mathrm{sat}}(\omega)$ data calculated by equation (40) for all doubly-excited states described in 2.3.2, including those with energies higher than

30.5 eV, for the prediction of strong resonance features in the satellite state spectra in the energy range from 30 to 33 eV. Since these features were not observed in the satellite state spectra with the threshold energy $\bar{E} < 30$ eV, they were assumed to lie in the cross section of the high-energy ($\bar{E} > 30$ eV) satellite levels.

4. Summary

The present paper is the fourth of a series of papers devoted to the experimental and theoretical study of the photoionization of the Kr atom for photon energies above the 4s-electron threshold. The complex energy dependence of various cross sections has been measured by using the PIFS method and the direct photoionization cross sections for the production of the Kr II 4s state and satellite states have been calculated by combining MBPT and CI techniques.

In the present paper we calculated the photoionization cross sections for the production of these states in the region of the 4s ionization threshold including for the first time the interference between the direct photoionization and the photoionization through the autoionization decay channels of doubly-excited states. A considerable number of doubly-excited states with energies between 27.06 eV and 30.65 eV were taken into account. A strongly structured energy dependence of the cross sections results from the calculations. The various interference effects which cause the appearance of fine-structure details and the redistribution of intensity in the calculated spectra are discussed. In the case of isolated resonances the calculated structures come very close to the experimental observation with respect to position and shape of the resonance. In particular the different shape of the resonance at 28.5 eV observed in the cross section for the production of the 4s-main state and of the satellite cross sections are reproduced by the new calculations. If, however, many resonances are present in a narrow energy range the calculated energy dependence of the cross section agrees with the experimental one only in the coarse features. The agreement may be improved by including an enlarged set of doubly-excited states of configurations with np-($n > 6$) and nf-electrons and by taking into account also the mutual interaction of the np/nf-electrons with core electrons.

A two-step model for the resonance enhancement of the 4s-photoionization cross section and the satellite production was investigated. The model, in which the excitation to doubly excited states and the decay of these states are considered to be independent of each other and of direct photoionization, enables us to describe satisfactorily the photoionization of satellite levels. On the basis of the two-step model calculations, the strong resonance features in the cross sections for the satellite levels with threshold energies $\bar{E} > 30$ eV are predicted.

Acknowledgments

This work has been funded by the German Federal Minister for Research and Technology under contract no 05 5UKAXB. BML and VLS gratefully acknowledge support by the Department of Physics, University of Kaiserslautern during their stay at Kaiserslautern.

References

Åberg T and Howat G 1982 *Theory of Auger effect* (*Encyclopedia of Physics* vol 31) ed S Flügge (Berlin: Springer) pp 469–619

Aksela S, Aksela H, Levasalmi M, Tan K H and Bancroft G M 1987 *Phys. Rev.* A **35** 3449–50

Amusia M Ya and Cherepkov N A 1975 *Case Stud. At. Phys.* **5** 47–121

Combet-Farnoux F 1982 *Phys. Rev.* A **25** 287–303

Ehresmann A, Vollweiler F, Schmoranzer H, Sukhorukov V L, Lagutin B M, Petrov I D, Mentzel G and Schartner K H 1994 *J. Phys. B: At. Mol. Opt. Phys.* **27** 1489–96

Fano U 1961 *Phys. Rev.* **124** 1866–78

Hall R I, Avaldi L, Dawber M and King G C 1990 *J. Phys. B: At. Mol. Opt. Phys.* **23** 469–85

Mies F H 1968 *Phys. Rev.* **175** 164–75

Moore C E 1971 *Atomic Data Levels* (NBS Circular No 467) (Washington, DC: US Govt Printing Office)

Schmoranzer H, Ehresmann A, Vollweiler F, Sukhorukov V L, Lagutin B M, Petrov I D, Schartner K H and Möbus B 1993 *J. Phys. B: At. Mol. Opt. Phys.* **26** 2795–810 (Corrigendum 1994 *J. Phys. B: At. Mol. Opt. Phys.* **27** 377–9)

Schmoranzer H, Wildberger M, Schartner K H, Möbus B and Magel B 1990 *Phys. Lett.* **150A** 281–5

Smid H and Hansen J E 1983 *J. Phys. B: At. Mol. Phys.* **16** 3339–70

Starace A F 1977 *Phys. Rev.* A **16** 231–42

Sugar J and Musgrove A 1991 *J. Phys. Chem. Ref. Data* **20** 859–916

Sukhorukov V L, Lagutin B M, Petrov I D, Schmoranzer H, Ehresmann A and Schartner K H 1994 *J. Phys. B: At. Mol. Opt. Phys.* **27** 241–56

Wills A A, Cafolla A A, Comer J 1990 *J. Phys. B: At. Mol. Opt. Phys.* **23** 2029–36